



## Synthesis and Characterization of ZnO Nanostructures Grown via a Novel Atmospheric Pressure Solution Evaporation Method

Mehdi Hamdam Momen<sup>\*</sup>, Mahmoud Heydarzadeh Sohi and Ahmadali Amadeh

*School of Metallurgy and Materials Engineering, College of Engineering, University of Tehran, P.O. Box 11155-4563, Tehran, Iran*

Received: 14 February 2015; Accepted: 29 June 2015

<sup>\*</sup>Corresponding Author Email: [mehdihamdamm@ut.ac.ir](mailto:mehdihamdamm@ut.ac.ir), Tel: +98(21)82084609, Fax: +98(21)88006076

### ABSTRACT

In this study, a novel method called “atmospheric pressure solution evaporation (APSE)” was developed for growing of Zinc Oxide (ZnO) nanostructures on Al<sub>2</sub>O<sub>3</sub> surface. Zinc acetate dihydrate, Polyvinyl Pyrrolidone, and deionized water were used as precursor, capping, and solvent, respectively. The growth of ZnO nanostructures from evaporated solution was performed at three temperatures of 300, 400, and 500°C. Field emission scanning electron microscopy (FESEM) demonstrated that ZnO nanostructures formed in nanorods or cauliflower-like rods based on the growth temperature. X-ray diffraction patterns of ZnO nanostructures prepared at different growth temperatures were indexed as hexagonal Wurtzite structure without any impurity. The optical band gap energy evaluated by diffuse reflectance spectroscopy (DRS) was 3.22~3.29 eV. Optical properties of the ZnO nanostructures are investigated by UV–Vis spectroscopy. There is a blue shift in the band edge with changing of the growth temperature. The degradation of Methylene Blue (MB) dye demonstrated that ZnO nanorods grown at the growth temperature of 300°C showed better photodegradation compared to other nanostructures. Antifungal properties of ZnO nanorods against *Candida albicans* were much higher than that of the other nanostructures. This method, compared to other synthesis methods of ZnO nanostructures, offers several advantages, such as simplicity, cost-effectiveness, low-temperature, atmospheric pressure, and large area deposition. Such a low-temperature growth method may expose great opportunities for synthesis of ZnO nanorods onto various low-temperature-endurance substrates and extend the field of ZnO-based nanoscale devices.

**Keywords:** *antifungal, atmospheric pressure solvent evaporation (APSE), growth temperature, photodegradation, ZnO nanostructures.*

### 1. Introduction

Zinc Oxide (ZnO) is extensively used in photodegradation of toxic organic pollutants and solving environmental problems due to its wide direct band gap (3.37 eV) and large

excitation binding energy (60 meV). Furthermore, ZnO, as a non-toxic and inexpensive material, has presented good mechanical, chemical, thermal, and photoetch stability [1, 2]. The use of ZnO as antibacterial

and antifungal agent has the advantages of improved safety and stability as compared to organic antimicrobial agents [3] which makes it appropriate for use in food industries, water and wastewater treatment, etc.

According to the published reports, nanosized powder ZnO presents higher photocatalytic and antimicrobial activity compared to bulk ZnO. Different morphologies of ZnO nanostructures, such as nanoparticles, nanorods, nanowires, nanotubes, nanobelts, nanoribbons, and nanosheets, were synthesized by various physical and chemical preparation methods [4-7]. These methods require high temperature, high purity precursors, high vacuum or difficult synthesis process.

In this research, a simple novel method called "atmospheric pressure solution evaporation (APSE)" was developed for synthesis of highly crystalline ZnO nanostructures and the effect of growth temperature on photocatalytic and antifungal properties was studied. This method, compared to other synthesis methods, offers several advantages such as simplicity, cost-effectiveness, low-temperature, atmospheric pressure, and large area deposition.

## 2. Experiment

Zinc Oxide nanostructures were grown on the basis of a novel atmospheric pressure solution evaporation method [8]. The growth of ZnO nanostructures from evaporated solution was performed on  $\text{Al}_2\text{O}_3$  surface at three temperatures of 300, 400, and 500°C. Thin films of  $\text{Al}_2\text{O}_3$  were prepared on glass substrates via dip coating process. For this purpose, alumina powder (KMS-92, Martinswerk) was suspended in deionized water and stirred for 24 hours. The glass substrates were then dip-coated by thin

alumina layers at immersing speed of 1 cm/min. The alumina coated glasses were then dried in an oven at 60°C for 12 hours.

Zinc Oxide nanostructures were grown on  $\text{Al}_2\text{O}_3$  layer by solution evaporation method. The solution was prepared by dissolving zinc acetate dehydrate (Merck) in deionized water (0.22 M). Polyvinylpyrrolidone (PVP) (Merck) was added as a surfactant with weight ratio of 1:10 of PVP: Zn. The solution was placed on a heater and stirred until the solution temperature reached 70 °C. The solution was heated at 70°C until the volume of solution was reduced to one-third of its initial volume and a small amount of zinc acetate and PVP gel was obtained. This solution was poured into a ceramic crucible and the coated substrates were placed on top of it. The ceramic crucible was then placed into an electric furnace. The samples were heated at a rate of 3°C/ min to 300, 400 and 500°C, respectively and cooled down to room temperature. Schematic of the growth process of ZnO nanorods on  $\text{Al}_2\text{O}_3$  substrate is shown in Figure 1.

Field emission scanning electron microscopy (FE-SEM, S4160 Hitachi Japan) was used to study the microstructure and morphology of the samples. The phase structure and crystallite size of grown nanostructures were investigated by X-ray diffraction technique (XRD, Philips Expert-MPD) using Cu-K $\alpha$  radiation with wavelength of 1.5439Å. The crystallite size of ZnO nanostructures was measured according to Scherrer equation [ $D=0.94\lambda/\beta \cos \theta$ ] where  $\lambda$  is the wavelength of X-ray,  $\beta$  is full width at half maximum intensity (FWHM) in radians and  $\theta$  is the Bragg angle. The specific surface

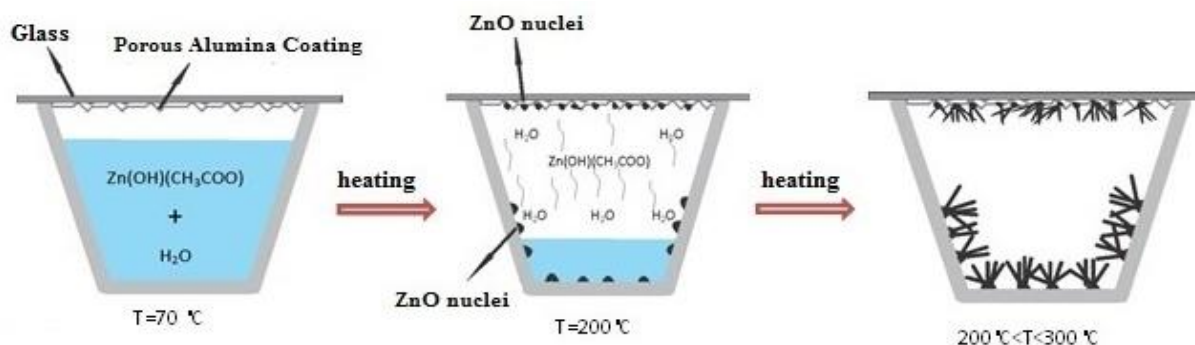


Fig. 1. The Scheme of the growth process

area was measured by nitrogen adsorption at  $-195.8^{\circ}\text{C}$  using the BET equation (Physisorption Analyzer, ASAP 2020, Micromeritics).

The optical characteristics of samples were analyzed by UV-Vis spectroscopy using the wavelength range of 190–1000 nm and diffuse reflectance spectra (DRS). To investigate the photocatalytic activity of the samples, the prepared ZnO nanostructures grown on  $\text{Al}_2\text{O}_3$  coated substrate were placed in a petri dish containing 10 ml of 5 ppm aqueous solution of MB. The petri dish was placed in a homemade box. The sample was then irradiated by a UV source (Osram, 400 W high-pressure Hg lamp) with prominent emission at 365 nm. The distance of lamp from reaction system was 1 cm and the temperature was fixed at  $25^{\circ}\text{C}$ . After UV-radiation, the concentration of MB solution was measured by UV-Visible spectrophotometer (Hitachi U-2000). The change in the concentration of MB was measured at regular intervals of time.

### 3. Results and Discussion

#### 3.1. Morphological properties

FESEM images of the grown structures, shown in Figure 2, indicate that high-density ZnO nanostructures are successfully obtained on  $\text{Al}_2\text{O}_3$  substrates, i.e.  $\alpha\text{-Al}_2\text{O}_3$  provides appropriate sites for nucleation and growth of ZnO. As shown in Figure 2a, dense vertically aligned hexagonal urchin-shaped faceted nanorods with a diameter range of 30–70 nm grow at temperature of  $300^{\circ}\text{C}$  over a large area of the substrate. As the growth temperature increases (Figs. 2b and 2c), ZnO morphology changes from nanorod to a cauliflower-like structure. The size of cauliflower rods is in the range of 150–250 nm and 200–300 nm at 400 and  $500^{\circ}\text{C}$ , respectively. The density of cauliflower rods is decreased compared to Figure 2a. This evolution can be attributed to the difference in nucleation and growth mechanism of ZnO particles at different growth temperatures [8].

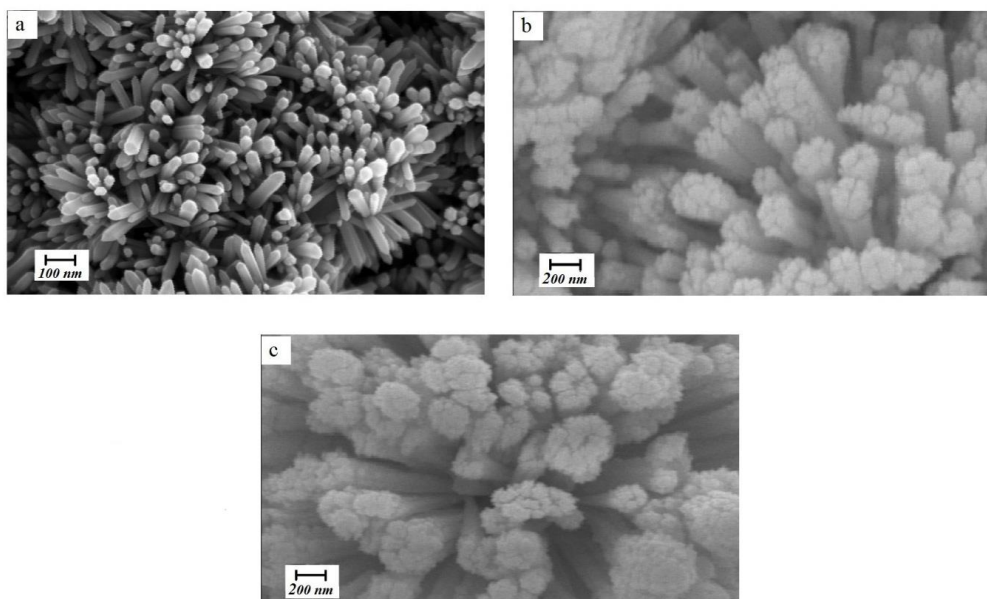


Fig. 2. FESEM images of ZnO structures grown on  $\alpha\text{-Al}_2\text{O}_3$  coated substrates at different growth temperatures: a)  $300^{\circ}\text{C}$ ; b)  $400^{\circ}\text{C}$  and c)  $500^{\circ}\text{C}$

#### 3.2. Structural properties

Figure 3 shows X-ray diffraction patterns of ZnO nanostructures prepared at different growth temperatures. All diffraction peaks can be indexed as hexagonal Wurtzite structure without any impurity (ICSD75-0576,  $a = 3.242 \text{ \AA}$ ,  $c = 5.194 \text{ \AA}$ ). The strong intensity of (002) peak in Figure 3 indicates the high crystalline

quality as well as the highly oriented nature of ZnO nanorods.

It is reported that the intensity ratio of (002) polar planes to (100) nonpolar planes ( $I(002)/I(100)$ ) can influence the photocatalytic activity because the polar planes of ZnO help the formation of oxygen vacancies [9]. According to XRD results, when the growth temperature is

300 °C, the intensity of (002) peak is higher than (100) peak, which means that c-axis growth is dominant [10]. However, when the growth temperature increases, the preferred growth direction changes progressively to (100) direction, showing that the growth mode changes from one-dimensional (1D) growth to two-dimensional (2D) growth. Moreover, according to Figure 3, the full width at half maximum (FWHM) of diffraction peaks decreases as the growth temperature increases. So, based on the Scherrer equation [7], a finer crystallite size can be expected at 300°C with respect to 400 and 500°C which confirms the result of FESEM micrographs. The crystallite size of synthesized structures calculated from Scherrer equation is presented in Table 1.

The results of specific surface area measurements are also shown in Table 1. As the growth temperature is increased, the BET specific surface area decreases. A high specific surface area increases the number of active sites on the surface of photocatalyst which leads to a faster reaction rate of photogenerated charge carriers, and so improves the efficiency of photocatalytic degradation of organic pollutants [11].

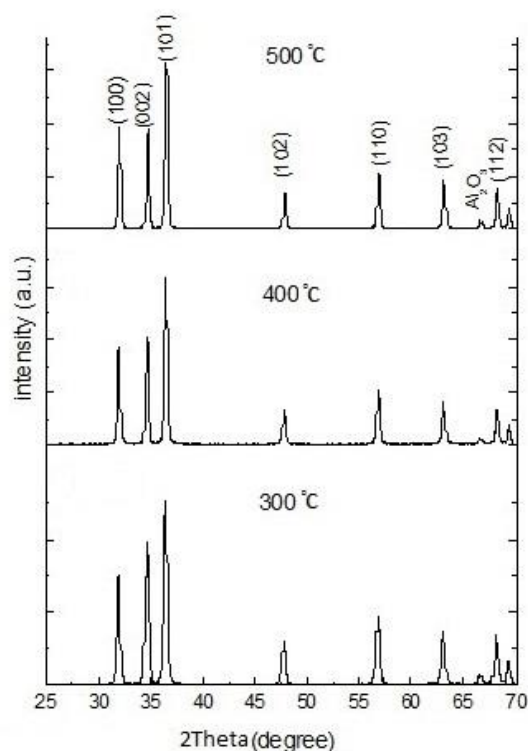


**Fig. 3.** XRD patterns of ZnO nanostructures ZnO nanostructures grown on  $\alpha$ - $\text{Al}_2\text{O}_3$  coated substrates at different temperatures of 300; 400 and 500°C

**Table 1.** The mean crystallite size, ratio of (002) plane to (100) plane and surface area of ZnO samples

Growth temperature (°C)	Mean crystallite size (nm)	I (002)/I (100)	BET surface area ( $\text{m}^2/\text{g}$ )
300	45	1.28	10.07
400	59	1.10	6.71
500	67	0.91	5.43

### 3.3. Photodegradation process

The photodegradation of Methylene Blue (MB) is defined as the normalized change in its concentration ( $C/C_0$ ) (Fig. 4). From this figure, it can be seen that ZnO nanorods prepared at growth temperature of 300°C exhibit the highest photocatalytic efficiency. Photocatalytic reactions take place at the interface between the catalyst and the organic pollutants [12]. Because the nanorods have higher surface area than the cauliflower-like structures, and the electron transport is easier in an interconnected structure than in a lumped one [12], the photocatalytic property of ZnO nanorods is superior than other nanostructures.

### 3.4. UV-VIS absorption spectra

The band gap energy ( $E_g$ ) of ZnO nanostructures can be calculated from the UV-Vis spectra by Tauc plot of  $(h\nu\alpha)^2$  versus  $(h\nu)$  and extrapolation of the linear portions of curves to energy axis according to Equation (1) [13, 14]:

$$(h\nu\alpha)^2 = A(h\nu - E_g) \quad (1)$$

where  $h\nu$  is photon energy,  $\alpha$  is absorption coefficient,  $E_g$  is direct band gap energy, and  $A$  is proportional constant. Normally the obtained diffuse reflectance spectrum is converted to Kubelka-Munk function in which  $\alpha$  in Tauc equation is substituted with  $F(R_\infty)$  according to Equation (2) [14].

$$(h\nu F(R_\infty))^2 = A(h\nu - E_g) \quad (2)$$

The diffuse reflectance spectra were analyzed using Kubelka-Munk function. This function  $F(R_\infty)$  is related to the diffuse reflectance  $R_\infty$  of the sample by Equation (3).

$$F(R_\infty) = \frac{(1-R)^2}{2R} \quad (3)$$

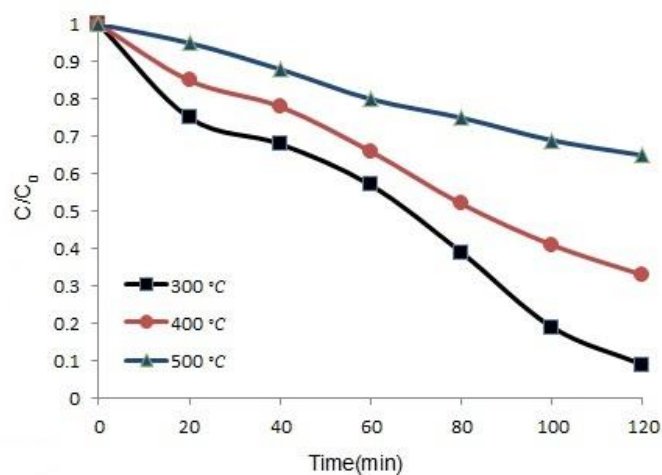


Fig. 4. photodegradation of MB aqueous solution degraded by ZnO nanostructures under UV light. ZnO nanostructures grown on  $\alpha$ - $Al_2O_3$  coated substrates at different temperatures of 300; 400 and 500°C

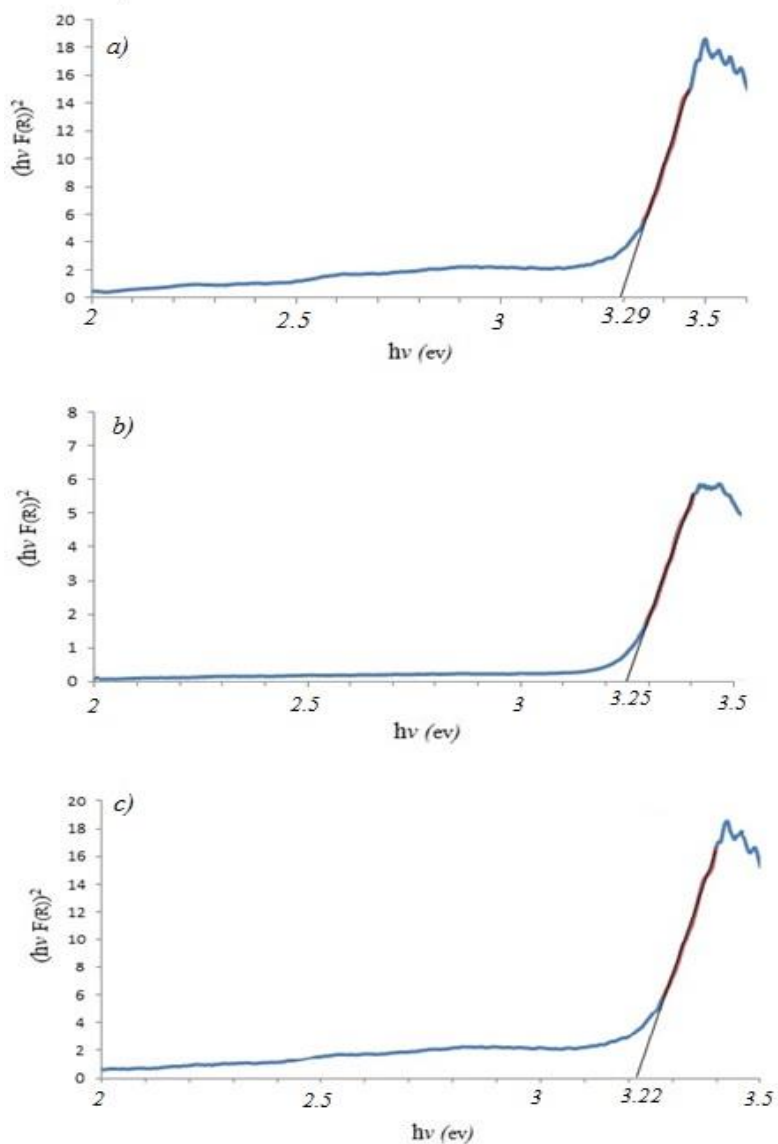


Fig. 5. Tauc plot of ZnO nanostructures at different growth temperatures: a) 300; b) 400 and c) 500°C

Here,  $R_{\infty}$  is the absolute value of reflectance and  $F(R_{\infty})$  is equivalent to the absorption coefficient. Hence, according to Equation (2), the indirect band gap of ZnO nanostructure was estimated by plotting  $(h\nu F(R_{\infty}))^2$  versus  $h\nu$  in Figure 5.

The estimated optical band gaps of ZnO nanostructure synthesized at the growth temperatures of 300, 400, and 500 °C are about 3.29 eV, 3.25 eV, and 3.22 eV, respectively. The position of the absorption spectra of ZnO sample synthesized at 300°C is observed to shift towards the lower wavelength side compared to the other two growth temperatures. The blue shift indicates the decrease in size of the particle and increase in band gap energy [15]. The increase in the band gap or blue shift clearly explains the quantum confinement effect of ZnO nanostructures. In addition, the blue shift of absorption edge can possibly be attributed to higher defect density on the surface of nanostructures with lower diameters. Different defect concentrations are expected to provide new bound excitons with new binding

energies which can result in spectral shift in nanostructures with different sizes [16].

### 3.5. Antifungal properties

To study the antifungal properties, *Candida albicans* primary was cultured on Sabouraud dextrose agar medium. Yeast cells were counted and adjusted at  $1 \times 10^6$  cell/mL by using Neubauer slide. The antifungal activity test of ZnO nanorods against *Candida albicans* under UV irradiation was evaluated by broth microdilution technique. It was observed that the prepared nanostructures diminish and inhibit the growth of cells (inhibitor zone around the disk) (Figure 6). Comparing the cell concentration on control substrate and ZnO nanostructures grown on  $Al_2O_3$  substrate shows the highest antifungal activity of ZnO nanorods prepared at 300°C.

Considering the fact that ZnO nanostructures can also eliminate the fungi cells without UV irradiation, the antifungal activity of ZnO is due to the generation of highly reactive oxygen species such as  $OH^{\cdot}$ ,  $O_2^{2-}$  and  $H_2O_2$  as well as mechanical damage of the cell membrane [3, 17].

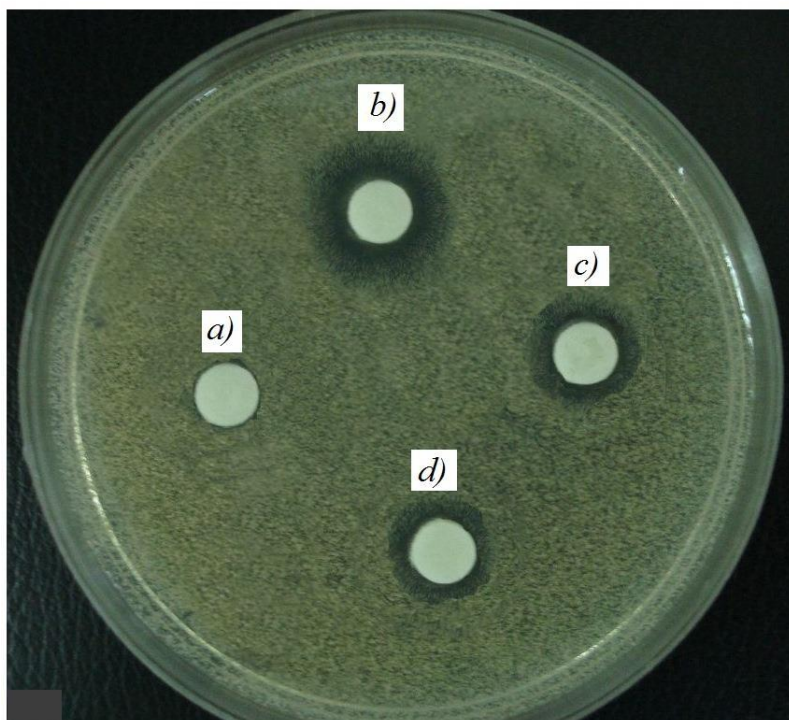


Fig. 6. Optical image of the grown cells around the plates including the antifungal nanostructures: a) blank control and plate treated by the grown nanostructure at b) 300; c) 400 and d) 500°C

#### 4. Conclusions

Zinc Oxide nanostructures were synthesized on  $\alpha$ -Al<sub>2</sub>O<sub>3</sub> substrate via a simple novel method called “atmospheric pressure solution evaporation (APSE)” at 300, 400, and 500°C. The growth temperature plays a significant role on morphology evolution of the grown products from nanorods to cauliflower-like structures. The X-ray diffraction patterns of ZnO nanostructures can be indexed as hexagonal Wurtzite structure without any impurity. According to XRD results, when the growth temperature is 300°C, the intensity of (002) peak is higher than (100) peak, which means that c-axis growth is dominant. However, when the growth temperature increases, the preferred growth direction changes to (100) direction, showing that the growth mode changes from 1D growth to 2D growth. The estimated optical band gaps of ZnO nanostructure synthesized at the growth temperatures of 300, 400 and 500 °C are about 3.29 eV, 3.25 eV and 3.22 eV, respectively. ZnO nanorods prepared at 300 °C exhibited the highest photocatalytic and antifungal activity.

#### References

- [1]. Nair, M. G., Nirmala, M., Rekha, K., Anukaliani, A., *Mater. Lett.* Vol., 65 (2011) pp. 1797 –1800.
- [2]. Zhang, H., Feng, J., Wang, J., Zhang, M., *Mater. Lett.*, Vol. 61 (2007) pp. 5202 – 5205.
- [3]. Manna, A. C., (In N. Cioffi, & M. Rai (Eds.), *Nano-Antimicrobials: Synthesis, Characterization, and Antimicrobial Activity of Zinc Oxide Nanoparticles* (2012) p. 151-180, New York: Springer).
- [4]. Liu, C., Li, H, Jie, W., Zhang, X., Yu, D. , Preparation of ZnO cluster and rod-like whiskers through hydrothermal methods. *Mater. Lett.*, Vol. 60 (2006) pp. 1394–1398.
- [5]. Liu, J. P., Huang, X. T., Duan, J. X., Ai, H. H., Tu, P. H., *Mater. Lett.*, Vol. 59 (2005) pp. 3710-3714.
- [6]. Breedon, M., Rahmani, M. B., Keshmiri, S. H., Wlodarski, W., Kalantar-zadeh, K., *Mater. Lett.*, Vol. 64 (2010) pp. 291 –294.
- [7]. Eskandari, M., Ahmadi, V., Ahmadi, S. H., *Physica B*, Vol. 404 (2009) pp. 1924-1928.
- [8]. Hamdam Momen, M., Amadeh, A., Heydarzadeh Sohi, M., Moghanlou, Y., *Mater. Sci. and Eng. B*, Vol. 190 (2014) pp. 66-74.
- [9]. Li, G., Hu, T., Pan, G., Yan, T., Gao, X., Zhu, H., *J. Phys. Chem. C*, Vol. 112 (2008) pp. 11859-11864.
- [10]. Fang, Y., Wang, Y., Wan, Y., Wang, Z., Sha, J., *J. Phys. Chem. C*, Vol. 114 (2010) pp. 12469-12476.
- [11]. Habibpanah, A. A., Pourhashem, S., Sarpoolaky, H., *J. Eur. Ceram. Soc.*, Vol. 31 (2011) pp. 2867-2875.
- [12]. Kim, S. J., Park, D. W., *Appl. Surf. Sci.*, Vol. 255 (2009) pp. 5363-5367.
- [13]. Anderson, C., Bard, A. J., *J. Phys. Chem. B*, Vol. 101 (1997) pp. 2611-2616.
- [14]. Simmons, B. A., Li, S., John, V. T., McPherson, G. L., Bose, A., Zhou, W., He, J., *Nano Lett.*, Vol. 2 (2002) pp. 263–268.
- [15]. Saravanan, R., Thirumal, E., Gupta, V.K., Narayanan, V., Stephen, A., *J. Mol. Liq.*, Vol. 177 (2013) pp. 394 –401.
- [16]. Djurišić, A. B., Leung, Y. H., *Small*, Vol. 2 (2006) pp. 944-961.
- [17]. Padmavathy, N., Vijayaraghavan, R., *Sci. Technol. Adv. Mater.*, Vol. 9 (2008) pp. 035004-035010.